IEEE Access
Multidisciplinary ⋮ Rapid Review ⋮ Open Access Journal

Received 17 February 2023, accepted 17 March 2023, date of publication 27 March 2023, date of current version 31 March 2023.

Digital Object Identifier 10.1109/ACCESS.2023.3261902

RESEARCH ARTICLE

Analytical Study and Noise Mitigation for Complex-Valued Optical DSB Transmission With Carrier-Assisted Differential Detection Receiver

PENG QIN[1], CHENGLIN BAI[1,2,3], (Senior Member, IEEE), QI QI[1], HENGYING XU[1,2,3], FAN YANG[1], PENGFEI LI[1], AND YINING ZHANG[4]

[1]School of Physics Science and Information Engineering, Liaocheng University, Liaocheng 252000, China
[2]Shandong Provincial Key Laboratory of Optical Communication Science and Technology, Liaocheng 252000, China
[3]Liaocheng Key Laboratory of Industrial-Internet Research and Application, Liaocheng 252000, China
[4]School of Mathematical Sciences, Liaocheng University, Liaocheng 252000, China

Corresponding authors: Chenglin Bai (baichenglin@lcu.edu.cn) and Hengying Xu (xuhengying@lcu.edu.cn)

This work was supported in part by the National Natural Science Foundation of China under Grant 61501213 and Grant 61671227; in part by the Shandong Provincial Natural Science Foundation under Grant ZR2020MF012, Grant ZR2020QF005, and Grant ZR2022MF253; and in part by the Doctoral Research Start-up Foundation of Liaocheng University under Grant 318051834 and Grant 318051835.

ABSTRACT A thorough analysis of the system model for complex-valued optical double-sideband (DSB) transmission with carrier-assisted differential detection (CADD) receiver under the influence of laser phase noise and fiber chromatic dispersion (CD) is presented. It is shown that the interaction of laser phase noise and CD leads to the phenomenon of phase-to-amplitude (P2A) noise and equalization-enhanced phase noise (EEPN). The achievable performance of the complex-valued optical DSB transmission with CADD receiver under the influence of EEPN and P2A noise is estimated by a closed-form expression, and it is verified by simulation that the results show an inaccuracy of less than 1 dB for a wide range of system parameters. In addition, in order to mitigate the EEPN and P2A noise, we propose a pre-decision aid-based simplified blind phase search (BPS) algorithm, commonly referred to as PDA-BPS algorithm. The PDA-BPS algorithm allows for reduced complexity by decreasing the number of symbols entering the BPS algorithm. Theoretical derivation and simulation verification illustrate that the PDA-BPS algorithm can achieve similar mitigation performance to the BPS algorithm with lower complexity. Specifically, under the condition that classification decision threshold R is equal to 0.25, the complexity can be reduced by 40%/16.6% with 1 MHz/7 MHz linewidth for 16-QAM and 29%/10.9% with 0.5 MHz/3 MHz linewidth for 64-QAM.

INDEX TERMS Carrier-assisted differential detection, equalization-enhanced phase noise (EEPN), laser linewidth, phase to amplitude noise (P2A), short-reach interconnects.

I. INTRODUCTION

Driven by 8K high-definition video, augmented/virtual reality (AR/VR), cloud computing, and other broadband services in 5G era, the growth of data capacity has gradually shifted from the core network of ultra-long distance transmission to the direction of short-reach and medium-reach metropolitan area networks [1], [2], [3]. Short-reach transmission requires many transceivers, which pays more attention to cost issues than long-reach transmission. Conventional intensity modulation and direct detection (IM/DD) has become the first choice for short-reach and medium-reach transmission because of its low cost and easy implementation [4], [5], [6]. However, it suffers from spectral fading problems due to the square-law detection of the photodetector, and thus hinders the transmission distance and data rate [7]. In recent years, the self-coherent scheme has been widely discussed because it breaks through this limitation [8], [9], [10], [11], [12], [13], [14].

So far, enormous efforts have been devoted to improving the self-coherent systems' transmission distance and spectral efficiency (SE). In 2013, Shieh group proposed a

The associate editor coordinating the review of this manuscript and approving it for publication was S. M. Abdur Razzak.

block-wise phase switch scheme to achieve optical field recovery of double-sideband (DSB) signals [15]. In order to obtain both the in-phase and quadrature components of the optical field, $\pi/2$ phase shift is applied on the signal or the optical carrier of the two consecutive blocks, leading to only 50% electrical SE with respect to single polarization coherent detection. In 2015, Zhang and co-workers proposed a twin-SSB modulation scheme to detect a complex-valued DSB signal, but the usage of optical bandpass filter (OBPF) with sharp edge roll-off at the receiver prevents its practical application [16]. The aforementioned problems prompt scientists to explore new solutions, and Shieh group proposed a scheme called carrier-assisted differential detection (CADD) recently [17]. Three output photocurrents from the CADD receiver are combined to retrieve the optical field of the complex-valued DSB signal without the use of a sharp-slope OBPF. In Ref. [18], the CADD receiver was experimentally demonstrated. To further simplify the structure of the CADD receiver, a symmetric scheme without using the single-ended photodiode (SPD) branch was proposed and numerically studied in Ref. [19]. Considering that the electrical dispersion compensation (EDC) is lower in cost and easier to be implemented than the optical compensation scheme [18], the CADD system mainly adopts EDC. To further reduce the costs, distributed feedback (DFB) lasers were adopted to replace high-cost external cavity lasers (ECL) without considering the effect of DFB laser's linewidth (LW) in the simulation to reduce the analysis complexity [19]. However, the influence of DFB lasers' wide linewidth, even reaching several MHz, a study of the influence of laser phase noise on the system performance is necessary.

In this paper, we analyze the impact of laser phase noise on the complex-valued optical DSB transmission with CADD receiver by considering the phenomena of phase-to-amplitude (P2A) noise conversion and equalization enhanced phase noise (EEPN). A frequency domain analysis reveals the origin of the EEPN, which results from the non-linear inter-mixing between the sidebands of dispersed signals and the noise sidebands of DFB lasers. Furthermore, P2A noise is caused by the interaction of fiber chromatic dispersion (CD) and laser phase noise in the direct current (DC) term. Both EEPN and P2A noise may cause non-negligible performance degradation. The achievable performance of the complex-valued optical DSB transmission with CADD receiver under the influence of EEPN and P2A noise is estimated by a closed-form expression, and it is verified by simulation that the results show an inaccuracy of less than 1 dB for a wide range of system parameters. In addition, the EEPN cannot be mitigated with any linear filter since it has almost an identical spectrum as the transmitted signal, so we propose a pre-decision aid-based simplified blind phase search (PDA-BPS) algorithm. The PDA-BPS algorithm allows for reduced complexity by decreasing the number of symbols entering the BPS algorithm and can achieve similar mitigation performance to the BPS algorithm [20] with lower complexity. Specifically, under the condition that classification decision threshold R is equal to 0.25, the complexity can be reduced by 40%/16.6% with 1 MHz/7 MHz linewidth for 16-QAM and 29%/10.9% with 0.5 MHz/3 MHz linewidth for 64-QAM.

The rest of this paper is organized as follows. In Section II, the origin and impact of EEPN and P2A noise on the CADD system are analyzed in detail. The principle of the proposed PDA-BPS algorithm is also introduced. Section III shows the simulation results and provides corresponding discussions. Finally, Section IV concludes the article.

II. SYSTEM MODEL AND PDA-BPS ALGORITHM

In Ref. [19], the theoretical derivation of the complex-valued optical DSB transmission with CADD receiver has been given, but the laser phase noise and fiber chromatic dispersion were neglected. It has been demonstrated that the EEPN originates from the interaction of laser phase noise and fiber chromatic dispersion [21], [22], [23], [24], [25], [26]. Besides, the P2A noise is also excited due to the interplay of laser linewidth, fiber chromatic dispersion and square-law detection in direct detection (DD) systems [27], [28], [29]. EEPN and P2A noise was studied for the case of the Kramers-Kronig (KK) system [29], [30], however, to the best of our knowledge, there is no report concerning its effect on the complex-valued optical DSB transmission with CADD receiver. Fig. 1 shows the system model under the influence of laser phase noise and fiber chromatic dispersion.

A. GENERAL ANALYSIS

At the transmitter end, the time-domain and frequency-domain expressions of the electric domain DSB signal are $S(t)$ and $S(f)$, respectively. After in-phase/quadrature (IQ) modulation, the optical signal is obtained. The stochastic baseband equivalent represents the emitted laser which can be written as $e^{j\varphi(t)}$ and $X(f)$ in time and frequency domains, respectively. $\varphi(t)$ is the laser phase noise which is a random Wiener process characterized by the laser linewidth $\Delta\nu$. By neglecting the impact of fiber loss and nonlinearity, the received optical signal can be written as $[A + S(t)]e^{j\varphi(t)} \otimes h(t)$, where A is the amplitude of the virtual carrier, $h(t)$ and e^{jkf^2} are time and frequency domain responses due to CD, respectively, and $\otimes$ represents the convolution operation. Where $k = \pi DLc/f_0^2$, D is dispersion coefficient, L is fiber length, c is the speed of light and f_0 is carrier frequency. The optical signal is equally split into upper and lower branches by the coupler, and the upper branch signal is delayed by an optical delay line (ODL) with a delay of τ. The delayed signal is sent to the 90° optical hybrid together with the lower branch signal from the coupler output, and the photocurrent I_1 and I_2 are obtained through the balanced photodiode.

$$I_1 = \frac{1}{2}\mathrm{Re}\left\{\left[[A + S(t)]e^{j\varphi(t)} \otimes h(t-\tau)\right]^* [A + S(t)]\, e^{j\varphi(t)} \otimes h(t)\right\} \quad (1)$$

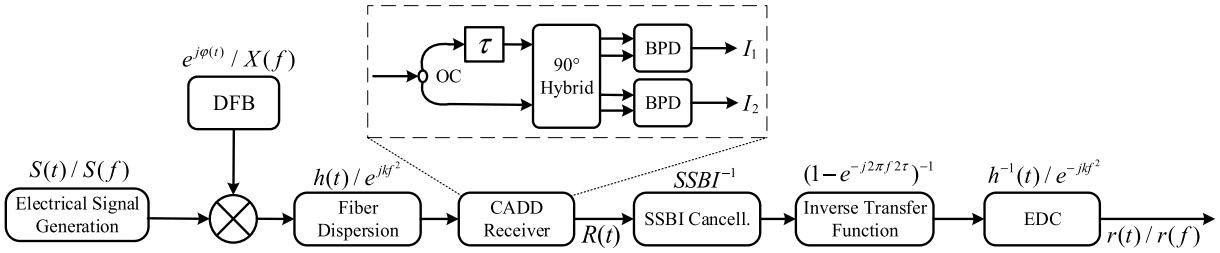

FIGURE 1. The system model of the optical DSB transmission with CADD receiver under the influence of laser phase noise and fiber chromatic dispersion. Inset: Structure of the CADD receiver; OC: optical coupler; BPD: balanced photodiodes.

$$I_2 = \frac{1}{2}\mathrm{Im}\left\{\left[[A+S(t)]e^{j\varphi(t)}\otimes h(t-\tau)\right]^* [A+S(t)]\,e^{j\varphi(t)}\otimes h(t)\right\} \quad (2)$$

Re $\{\cdot\}$ and Im $\{\cdot\}$ represent the real and imaginary parts, respectively. The optical field recovery can be realized by linearly combining the two photocurrents as

$$\begin{aligned} R_1(t) &= I_1 + jI_2 \\ &= \frac{1}{2}\left\{\left[Ae^{j\varphi(t)}\otimes h(t-\tau)\right]^*\left[Ae^{j\varphi(t)}\otimes h(t)\right]\right. \\ &\quad + \left[Ae^{j\varphi(t)}\otimes h(t-\tau)\right]^*\left[S(t)e^{j\varphi(t)}\otimes h(t)\right] \\ &\quad + \left[Ae^{j\varphi(t)}\otimes h(t)\right]\left[S(t)e^{j\varphi(t)}\otimes h(t-\tau)\right]^* \\ &\quad \left. + \left[S(t)e^{j\varphi(t)}\otimes h(t)\right]\left[S(t)e^{j\varphi(t)}\otimes h(t-\tau)\right]^*\right\} \quad (3) \end{aligned}$$

The delay τ can be applied to the waveform $R_1(t)$ as

$$\begin{aligned} R_1(t-\tau) &= \frac{1}{2}\left\{\left[Ae^{j\varphi(t)}\otimes h(t-2\tau)\right]^*\left[Ae^{j\varphi(t)}\otimes h(t-\tau)\right]\right. \\ &\quad + \left[Ae^{j\varphi(t)}\otimes h(t-2\tau)\right]^*\left[S(t)e^{j\varphi(t)}\otimes h(t-\tau)\right] \\ &\quad + \left[Ae^{j\varphi(t)}\otimes h(t-\tau)\right]\left[S(t)e^{j\varphi(t)}\otimes h(t-2\tau)\right]^* \\ &\quad + \left[S(t)e^{j\varphi(t)}\otimes h(t-\tau)\right] \\ &\quad \left.\times\left[S(t)e^{j\varphi(t)}\otimes h(t-2\tau)\right]^*\right\} \quad (4) \end{aligned}$$

By subtracting the conjugation of Eq. (4) from Eq. (3), the complex-valued signal $R(t)$ can be acquired as

$$\begin{aligned} R(t) &= R_1(t) - R_1^*(t-\tau) \\ &= \frac{1}{2}\left\{\left[Ae^{j\varphi(t)}\otimes h(t-\tau)\right]^*\right. \\ &\quad \times\left[Ae^{j\varphi(t)}\otimes h(t) - Ae^{j\varphi(t)}\otimes h(t-2\tau)\right] \\ &\quad + \left[Ae^{j\varphi(t)}\otimes h(t-\tau)\right]^* \\ &\quad \times\left[S(t)e^{j\varphi(t)}\otimes h(t) - S(t)e^{j\varphi(t)}\otimes h(t-2\tau)\right] \\ &\quad + \left[S(t)e^{j\varphi(t)}\otimes h(t-\tau)\right]^* \\ &\quad \times\left[Ae^{j\varphi(t)}\otimes h(t) - Ae^{j\varphi(t)}\otimes h(t-2\tau)\right] \\ &\quad + \left[S(t)e^{j\varphi(t)}\otimes h(t-\tau)\right]^* \\ &\quad \left.\times\left[S(t)e^{j\varphi(t)}\otimes h(t) - S(t)e^{j\varphi(t)}\otimes h(t-2\tau)\right]\right\} \quad (5) \end{aligned}$$

On the right-hand side of Eq. (5), the first term represents the P2A noise, the second term is the useful signal component, and the third term is the conjugate version of the second term. and the last term is signal-to-signal beating interference (SSBI). Due to the relatively small laser linewidth, the $Ae^{j\varphi(t)}\otimes h(t-\tau)$ approximated as $Ae^{j\varphi(t)}\otimes h(t)$. It is well-known that the CD converts the phase noise to amplitude noise [27], [30] as

$$Ae^{j\varphi(t)}\otimes h(t) \cong [A+n(t)]e^{j\varphi(t)} \quad (6)$$

where $n(t)$ represents the amplitude noise which is converted from the laser phase noise by the fiber CD. For explanation simplicity, we assume the SSBI could be mitigated by SSBI cancellation. Taking into account Eq. (6), the second term in Eq. (5) can be written as two items, one of which is P2A-signal beat (P2A-SB) noise with $n(t)$. The other item is converted to the frequency domain as shown below

$$\begin{aligned} r_2(f) &= \frac{1}{2}AX^*(f)\otimes\left[[S(f)\otimes X(f)]e^{jkf^2}[1-e^{-j2\pi f2\tau}]\right] \\ &= \frac{1}{2}AX^*(f) \\ &\quad \otimes\left[\int_{-\infty}^{\infty} S(f-f_1)X(f_1)e^{jkf^2}[1-e^{-j2\pi f2\tau}]df_1\right] \\ &= \frac{1}{2}A\left[\int_{-\infty}^{\infty}\int_{-\infty}^{\infty} S(f-f_1)X(f_1)\right. \\ &\quad \left.\times\, X^*(f_2)e^{jkf^2-2jkff_2+jkf_2^2}[1-e^{-j2\pi(f-f_2)2\tau}]df_1df_2\right] \end{aligned} \quad (7)$$

After the inverse transfer function module and electrical dispersion compensation, $r(f)$ is obtained.

$$\begin{aligned} r(f) = \frac{1}{2}A\left\{\int_{-\infty}^{\infty}\int_{-\infty}^{\infty} S(f-f_1)X(f_1)X^*(f_2)e^{jkf_2^2-2jkff_2}\right. \\ \left.\times[1-e^{-j2\pi(f-f_2)2\tau}]df_1df_2\right\}/[1-e^{-j2\pi f2\tau}] \end{aligned} \quad (8)$$

In Eq. (8), it can be found that $e^{jkf_2^2}$ will broaden the side band component of the signal due to the existence of the laser linewidth and fiber dispersion, but it is insignificant since the

linewidth is much smaller than signal bandwidth. We can also observe that e^{-2jkff_2} is almost parallel to signal spectrum and distributed within the whole signal band, it will cause the so-called EEPN. The inverse transfer function also affects the EEPN due to the non-exchangeable multiplication and convolution operations. Additionally, the EEPN cannot be mitigated with any linear filter since it has almost an identical spectrum as the transmitted signal. In this paper, we propose a PDA-BPS algorithm to mitigate its impacts as shown in 2.3.

B. THE NOISE CALCULATION

The EEPN induced noise scales linearly with the accumulated CD, laser linewidth and signal band width and it exists in the whole signal band. When the effect of the inverse transfer function on EEPN is ignored, the variance of the additional noise due to the EEPN can be described as [21]

$$\sigma^2_{EEPN} = \frac{A^2 P_S \pi \lambda_0^2 DLB_S \Delta v}{2c} \tag{9}$$

where B_S is the signal bandwidth, P_S is the signal power, and λ_0 is the center wavelength of the carrier. The normalized power spectral density of the P2A noise can be calculated by using a Bessel expansion of the electrical field and neglect contributions from the higher order terms.

According to [27] and [28], we can write the power spectral density (PSD) of the P2A as

$$N(f) = \frac{1}{2}\left\{\sum_{n=0}^{\infty} 4J_{\mathrm{n}}\left(\frac{1}{f}\sqrt{\frac{2\Delta v}{\pi}}\right)J_{\mathrm{n+1}}\left(\frac{1}{f}\sqrt{\frac{2\Delta v}{\pi}}\right) \times \sin\left[\frac{(2n+1)\pi c f^2 DL}{f_0^2}\right]\right\}^2 \tag{10}$$

where J_{n} is the Bessel function of the first kind. It is noted that to simplify the analysis, we assume that P2A and P2A-SB noise is signal-independent and is not affected by the inverse transfer function and EDC. Knowing the normalized noise spectral density, the noise power of the P2A noise interfering with signal is calculated as

$$\sigma^2_{P2A} = A^4 \int_{\Delta f/2}^{\Delta f/2+B_S} N(f)df \tag{11}$$

where Δf is the frequency gap between the left and right sideband signals. The total power of the beat noise between P2A and signal with a power of P_S can also be estimated as in Ref. [30]

$$\sigma^2_{P2A-SB} = A^2 P_S \int_{\Delta f/2}^{\Delta f/2+B_S} N(f)df \tag{12}$$

Assuming that SSBI is fully compensated, the signal-to-noise ratio (SNR) of the signal can be expressed as

$$SNR = \frac{A^2 P_S}{\sigma^2_{EEPN} + \sigma^2_{P2A} + \sigma^2_{P2A-SB}} \tag{13}$$

After simplification, the final SNR with the impact of ASE noise becomes

$$SNR = 1/\left\{\frac{\pi \lambda_0^2 DLB_S \Delta v}{2c} + (CSPR+1)\int_{\Delta f/2}^{\Delta f/2+B_S} N(f)df + \sigma^2_{ASE}\right\} \tag{14}$$

Eq. (14) shows the achievable performance of the CADD receiver based optical DSB transmission system. However, the SSBI in the CADD system cannot be eliminated entirely by iteration algorithm, and the inverse transfer function also interferes with the accuracy of the proposed model. In Section III, numerical simulations are implemented to investigate the achievable system performance.

C. THE PRINCIPLE OF THE PDA-BPS ALGORITHM

Fig. 2 shows the block diagram of the PDA-BPS algorithm. First, the received symbol r_k is fed into a pre-decision circuit which includes calculating the distances D_k between r_k and all ideal constellation points, and determining whether the minimum distance of D_k is less than a classification decision threshold R. (the size of R is an empirical value, which can be changed according to different situations and needs. In this case, the value of R is optimized in section III-C) If so, the symbol r_k is output directly. At this point, the influence of EEPN and P2A noise on the symbol can be ignored. If the minimum distance of D_k is greater than the threshold R, the received symbol r_k is rotated by multiple test phase angles φ_b with

$$\varphi_b = \frac{b}{B} \times \frac{\pi}{2}, b \in \{0, 1, \cdots, B-1\} \tag{15}$$

The parameter B is the number of test phase angles, and it is set to 18 and 28 for the 16-QAM and 64-QAM CADD systems, respectively, when mitigating EEPN and P2A noise. Then all rotated symbols are fed into a decision circuit, and the squared distance $\left|d_{k,b}\right|^2$ to the closest constellation point is calculated. In order to remove distortions from additive noise, the distances of N ($N = 16$ for 16-QAM and $N = 22$ for 64-QAM) consecutive test symbols rotated by the same phase angle φ_b are summed up

$$S_{k,b} = \sum_{n=-N}^{N} \left|d_{k-n,b}\right|^2 \tag{16}$$

The optimum phase angle is determined by searching the minimum sum of distance values. As the decoding is already executed in Eq. (15), the output phase angles φ_k can be selected from the φ_b using a switch controlled by the index of the minimum distance sum. The output phase angle is used to mitigate the effects of EEPN and P2A noise.

The constellations in Fig. 2(a) show the quality of the recovered 16-QAM signal at 300 km when the laser linewidth is 3 MHz. The combined action of EEPN and P2A noise leads to the rotation and dispersion of constellation points. Fig. 2(b) shows the constellation diagram after the PDA-BPS

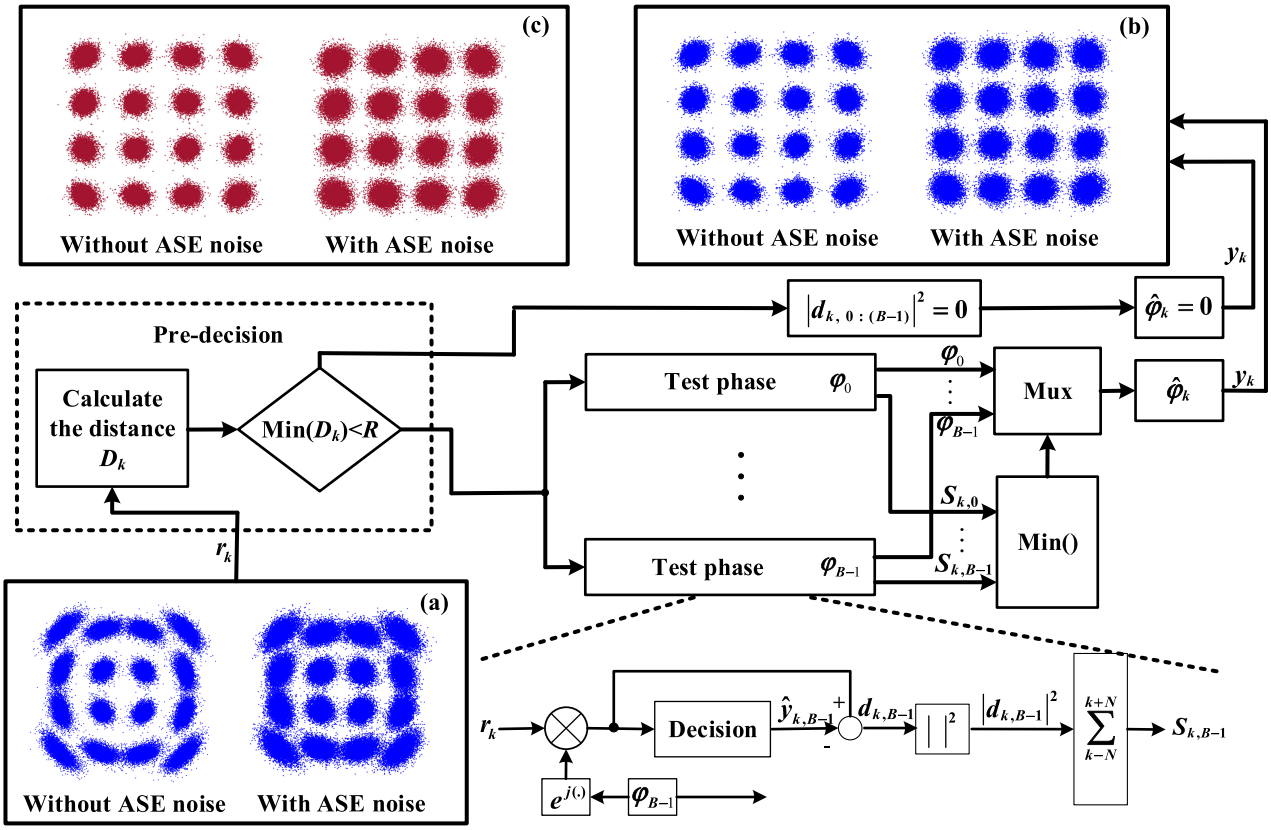

FIGURE 2. Block diagram of the proposed PDA-BPS algorithm. Inset: constellation of the 16-QAM symbols after 300 km transmission when the laser linewidth is 3 MHz (a) without algorithms; (b) with the proposed PDA-BPS algorithm; (c) with the BPS algorithm.

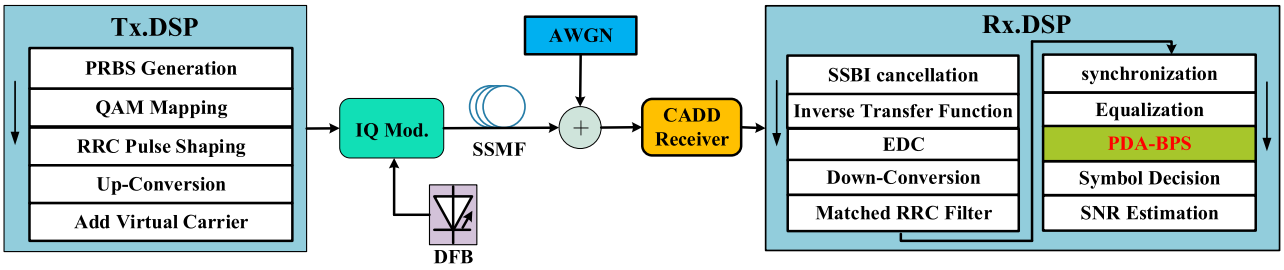

FIGURE 3. Simulation setup. IQ Mod.: IQ modulator; SSMF: standard single-mode fiber.

algorithm, and it can be found that the quality of the signal is significantly improved. In order to be able to demonstrate the superiority of the proposed algorithm, Fig. 2(c) shows the constellation diagram of the signal after mitigation by the BPS algorithm under the same conditions. The obtained results indicate that the quality of the signal after mitigation by the two algorithms is basically comparable. However, the proposed PDA-BPS algorithm has a lower complexity.

III. SIMULATION RESULTS AND ANALYSIS

A. SIMULATION SETUP

As shown in Fig. 3, the establishment of the optical DSB transmission with carrier-assisted differential detection receiver by co-simulation using MATLAB and VPI transmissionMaker11. 1 is accomplished. At the transmitter, the header of each frame has 1024 symbols for synchronization and equalization, and a total of 2^{17} bits are transmitted for the final BER calculation. The modulation format considers 16-QAM and 64-QAM. The two pseudo-random binary sequences (PRBS) bit streams are mapped to generate the symbol sequences that are pulse-shaped using root-raised cosine (RRC) filter with the roll-off of 0.01. And the signals are up-converted to obtain left and right sideband signals which are summed to obtain the twin-SSB signal. The transmitted optical signal is obtained by IQ modulation after adding the virtual carrier. Herein, the virtual carrier is used to facilitate the control of CSPR. The optical carrier is generated by a DFB laser, and the center frequency of

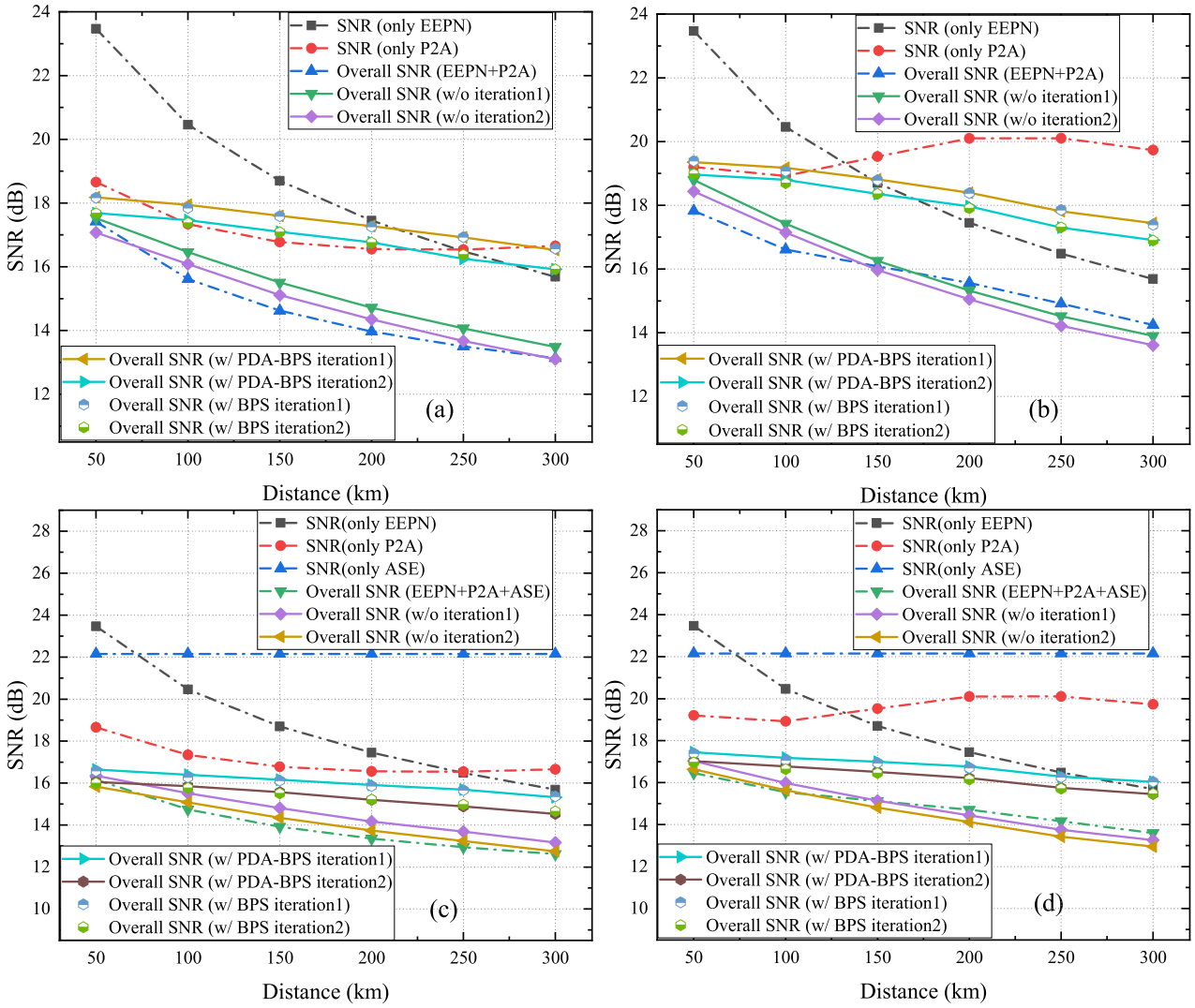

FIGURE 4. SNRs of 60 Gbaud 16-QAM CADD received signal after different transmission distance and the laser linewidth is 7 MHz. (a)Δf = 6GHz and without ASE noise; (b) Δf = 10GHz and without ASE noise; (c) Δf = 6GHz and with ASE noise; (d) Δf = 10GHz and with ASE noise. iteration1: SSBI simplified iteration cancellation algorithm; iteration2: SSBI complex iteration cancellation algorithm.

the optical carrier is set to 193.4 THz. Only the effects of CD and additive white Gaussian noise (AWGN) are considered in the channel, and the dispersion coefficient is set to 17 ps/nm/km. It should be noted that AWGN is accurately added by using a setting OSNR module in VPI. At the receiver side, the field recovery of the signal is achieved by using the CADD receiver. The optical delay in the receiver is set to 12.5 ps to keep the signal in the SSBI suppressed area. In order to eliminate SSBI as much as possible through iteration algorithm, the CSPR is set to 12 dB. And the Rx.DSP includes the SSBI cancellation, inverse transfer function, EDC, down-conversion, matched RRC filter, synchronization, equalization, PDA-BPS algorithm, symbol decision, and finally the SNR estimation module. The SSBI cancellation includes SSBI complex iterative elimination algorithm and SSBI simplified iterative elimination algorithm [19].

B. PERFORMANCE AND DISCUSSIONS

Since the transfer function of the CADD receiver is equivalent to that of a delay interferometer, the null point at zero frequency is inevitable. Thus, the SSBI and P2A noise are severely enhanced in the low-frequency region, which requires a frequency gap between the left and right sideband signals. A larger frequency gap can effectively suppress SSBI and P2A noise enhancement to increase the accuracy of the proposed model, but it will reduce the SE of the system. By weighing the pros and cons of SE and performance, while meeting the need to suppress SSBI and P2A noise, we consider the frequency gap of 6 GHz and 10 GHz to verify the accuracy of the proposed model. In addition, for in-depth research and analysis, we separately consider two cases including the existence of two kinds of noise (EEPN and P2A noise) and the existence of three kinds of noise

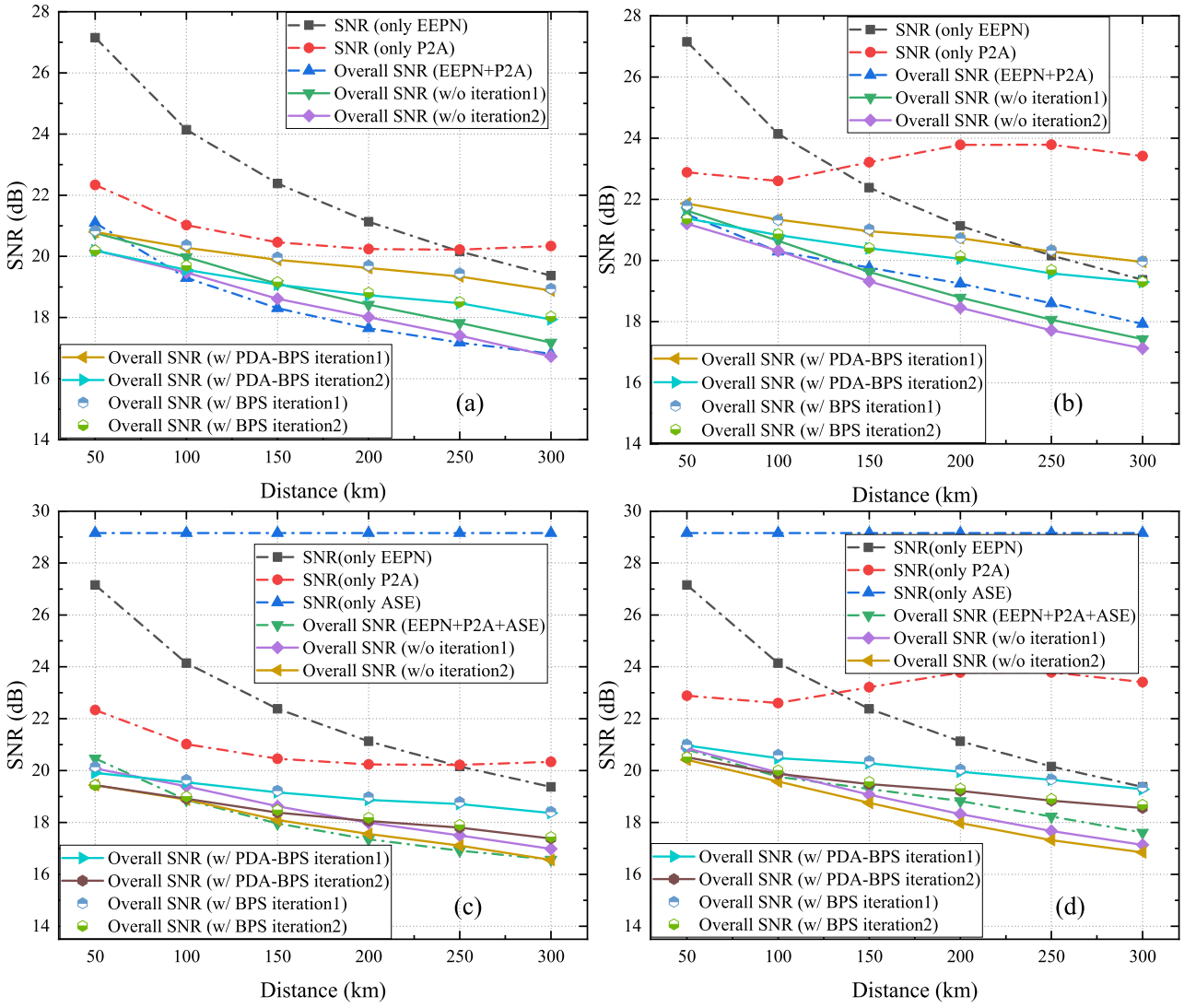

FIGURE 5. SNRs of 60 Gbaud 64-QAM CADD received signal after different transmission distance and the laser linewidth is 3 MHz. (a) Δf = 6GHz and without ASE noise; (b) Δf = 10GHz and without ASE noise; (c) Δf = 6GHz and with ASE noise; (d) Δf = 10GHz and with ASE noise.

(EEPN, P2A noise, and ASE noise) in the system. Specifically, Figs. 4-9 (a) and (b) only consider EEPN and P2A noise in order to focus on analyzing the mitigation effect of the proposed PDA-BPS algorithm on EEPN and P2A noise. In Figs. 4-9 (c) and (d), the ASE noise is also considered in order to be more realistic. However, due to the higher baud rate, the OSNR is set to 38 dB and 45 dB for the 16-QAM and 64-QAM modulation formats, respectively. Since the EEPN, P2A noise, and ASE noise are closely related to the three parameters (symbol rate, transmission distance and laser linewidth), we verify the proposed model by varying the three parameters. It is worth noting that according to the generation mechanism of EEPN and P2A noise, the two types of noise can be distinguished theoretically. Still, for the actual system, the two types of noise are generated at the same time, and the impact on system performance is manifested as a hybrid effect that cannot be precisely distinguished. There is no need to distinguish them, our mitigation algorithm can simultaneously equalize them.

Figs. 4 and 5 plot the SNR of the received signal at different transmission distances. The baudrate of the system is fixed at 60 Gbaud, and the linewidth of the DFB laser is fixed at 7 MHz/3 MHz for 16-QAM/64-QAM. All the dotted lines are theoretical calculation results and the rest are numerical simulation results. The obtained results indicate that the overall SNR decreases significantly as the transmission distances which attributes mainly to the increase of the EEPN. Meanwhile, the ASE noise and P2A noise change slightly with the increase in the transmission distance. In addition, the proposed PDA-BPS algorithm also significantly mitigates the influence of the increase in the transmission distance. This effectively extends the transmission distance of the CADD system. And it can be found that the proposed PDA-BPS algorithm has comparable mitigation performance compared

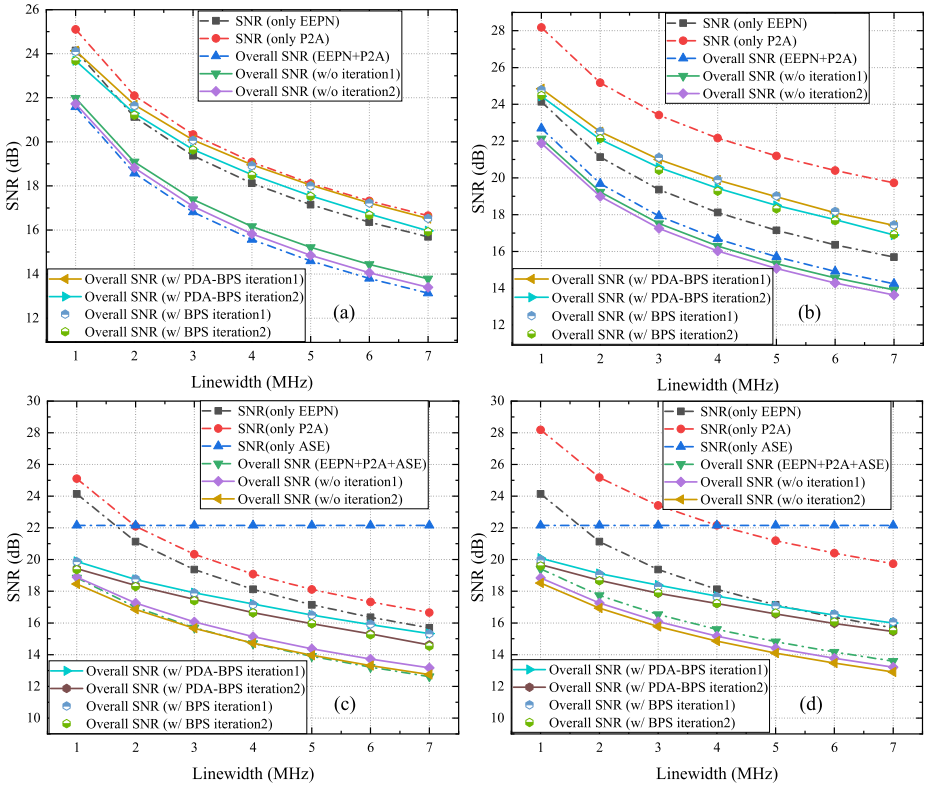

FIGURE 6. NRs of 60 Gbaud 16-QAM CADD received signal with different laser linewidth after 300 km transmission. (a) Δf = 6GHz and without ASE noise; (b) Δf = 10 GHz and without ASE noise; (c) Δf = 6GHz and with ASE noise; (d) Δf = 10GHz and with ASE noise.

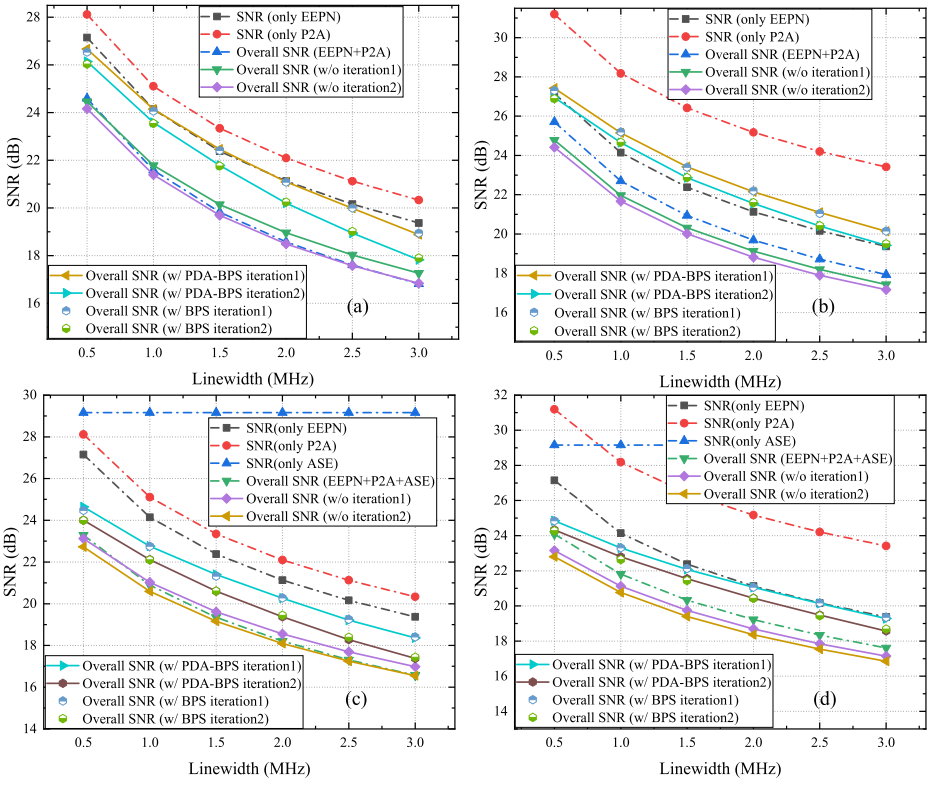

FIGURE 7. SNRs of 60 Gbaud 64-QAM CADD received signal with different laser linewidth after 300 km transmission. (a) Δf = 6GHz and without ASE noise; (b) Δf = 10 GHz and without ASE noise; (c) Δf = 6GHz and with ASE noise; (d) Δf = 10GHz and with ASE noise.

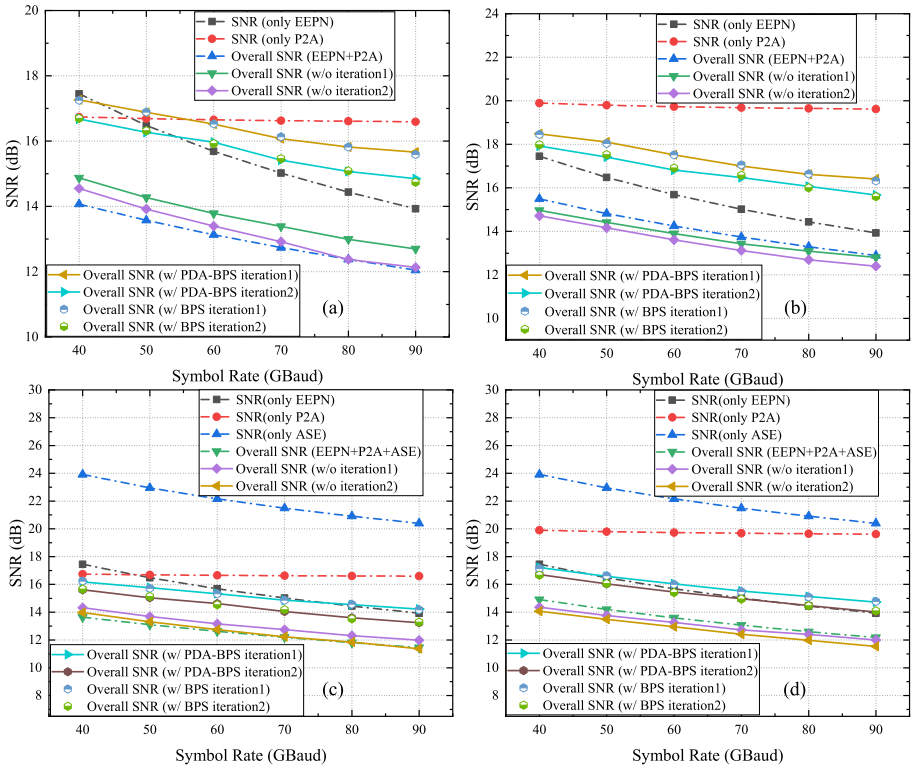

FIGURE 8. SNRs of 16-QAM CADD received signal with different symbol rate after 300 km transmission and the laser linewidth is 7 MHz. (a) $\Delta f = 6$GHz and without ASE noise; (b) $\Delta f = 10$GHz and without ASE noise; (c) $\Delta f = 6$GHz and with ASE noise; (d) $\Delta f = 10$GHz and with ASE noise.

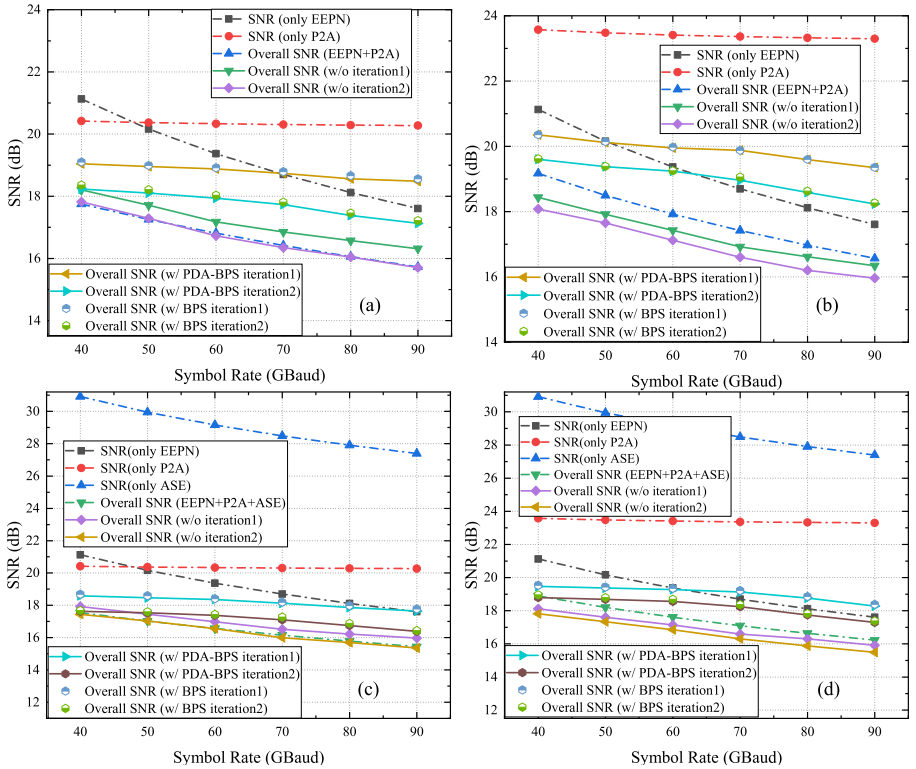

FIGURE 9. SNRs of 64-QAM CADD received signal with different symbol rate after 300 km transmission and the laser linewidth is 3 MHz. (a) $\Delta f = 6$GHz and without ASE noise; (b) $\Delta f = 10$GHz and without ASE noise; (c) $\Delta f = 6$GHz and with ASE noise; (d) $\Delta f = 10$GHz and with ASE noise.

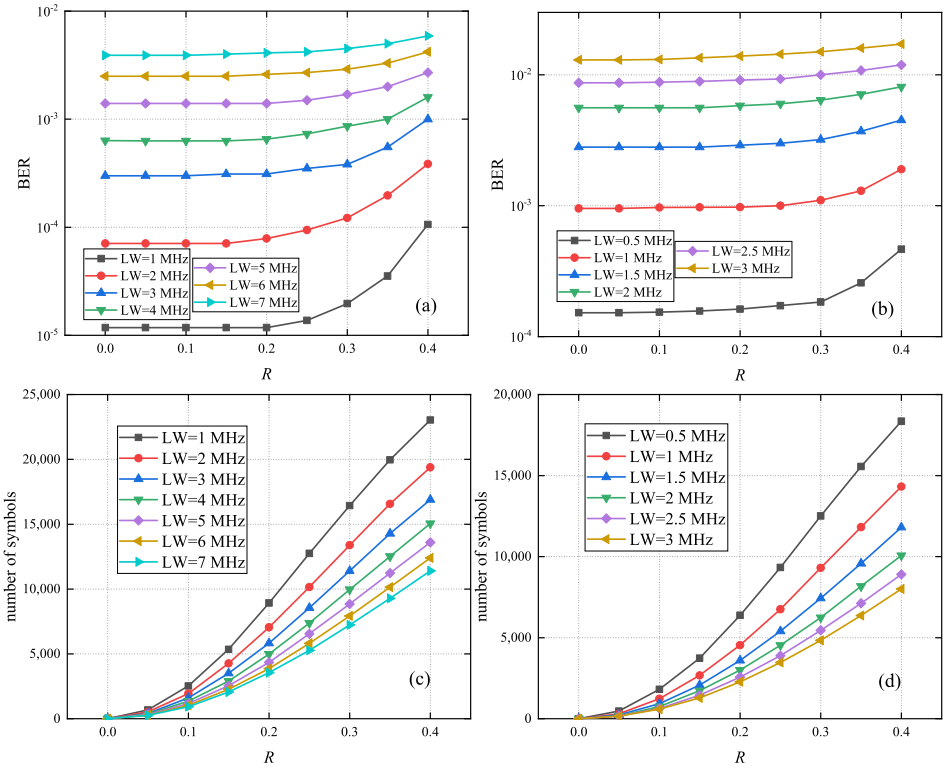

FIGURE 10. (a) BER performance versus R of different laser linewidths after 300 km transmission for 16-QAM. (b) BER performance versus R of different laser linewidths for 64-QAM. (c) number of N_2 versus R of different laser linewidths for 16-QAM. (d) number of N_2 versus R of different laser linewidths for 64-QAM.

with the BPS algorithm. However, the proposed PDA-BPS algorithm has a lower complexity. In the Figs.4-9 iteration1 represents SSBI simplified iteration cancellation algorithm, while iteration2 represents SSBI complex iteration cancellation algorithm. Under the combined effect of EEPN, P2A and ASE noise, the performance of SSBI simplified iteration elimination algorithm is better than SSBI complex iteration elimination algorithm.

Figs. 6 and 7 show the SNR of the 60 Gbaud 16-QAM and 64-QAM CADD received signals for different laser linewidths after 300 km transmission, respectively. We can find that: (1) The SNR of EEPN and P2A noise decreases significantly with the increasing of linewidth, and the SNR of ASE noise keeps constant. (2) With two kinds of noise in the system, by using the proposed PDA-BPS algorithm, the overall SNR is higher than the SNR of EEPN. These results imply that both EEPN and P2A noise are effectively mitigated. (3) Despite the fact that EEPN and P2A noise degrade the performance of the CADD system as a whole, the effectiveness of SSBI iterative cancellation algorithm is immune to the EEPN and P2A noise. (4) The proposed model and the PDA-BPS algorithm can be applied not only to 16-QAM, but also to higher-order 64-QAM modulation format. Additionally, considering that the 64-QAM modulation format is more sensitive to the linewidth, the maximum linewidth of 64-QAM is set to 3 MHz.

Figs. 8 and 9 show the SNR comparison between theoretical calculation and numerical simulation for 16-QAM and 64-QAM CADD systems after 300 km transmission with laser linewidth set to 7 MHz and 3 MHz for different values of the symbol rate, respectively. We can make the following conclusions: (1) The EEPN and P2A noise increase significantly with the increasing of symbol rate, while the ASE noise remains roughly constant. (2) The compensation effect of the proposed PDA-BPS algorithm is still obvious with the interference of ASE noise, and the performance of the proposed PDA-BPS algorithm is comparable to that of the BPS algorithm. Specifically, when the symbol rate is set to 90 Gbaud, the proposed PDA-BPS algorithm can improve the SNR from 11.9 dB to 14.7 dB under the SSBI simplified iterative elimination algorithm. (3) The P2A noise is significantly increased as Δf decreases from 10 GHz to 6 GHz, but it has no significant effect on the ASE noise and EEPN. (4) For all cases, the error of the proposed model is less than 1 dB by comparing the results of the theoretical calculations and numerical simulation.

C. COMPUTATIONAL COMPLEXITY

To clarify the superiority of the proposed PDA-BPS algorithm, whose complexity per symbol is compared with that of the BPS algorithm, as shown in Table 1. Herein, 16-QAM is taken as an example, because the reduction of complexity

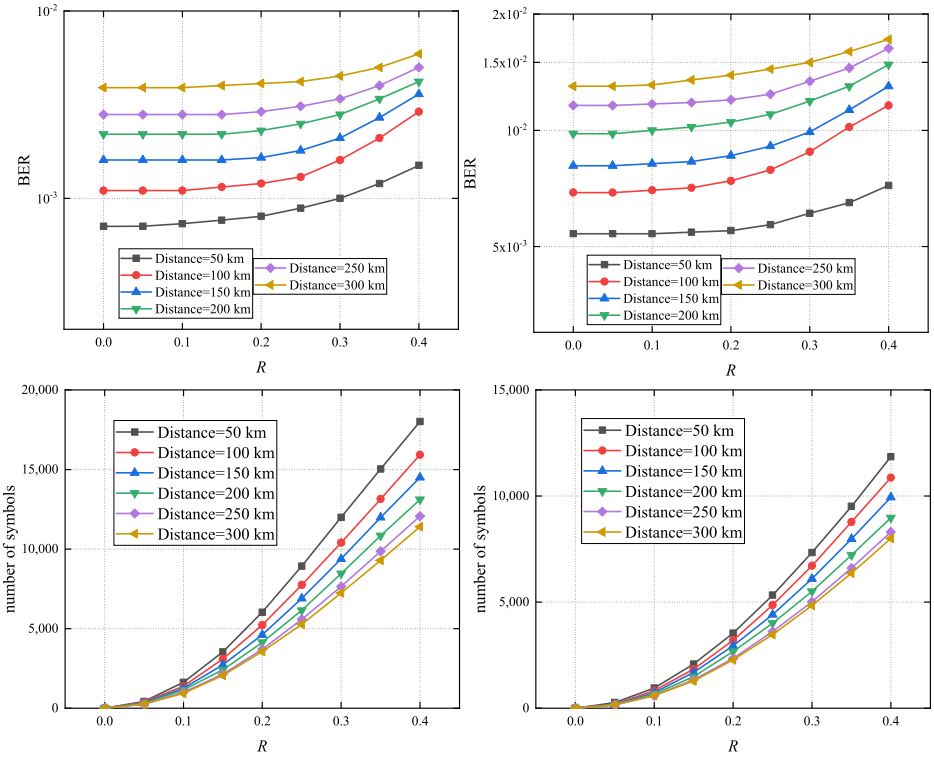

FIGURE 11. (a) BER performance versus R of different transmission distance for 16-QAM and the laser linewidth is 7 MHz. (b) BER performance versus R of different transmission distance for 64-QAM and the laser linewidth is 3 MHz. (c) number of N_2 versus R of different transmission distance for 16-QAM and the laser linewidth is 7 MHz. (d) number of N_2 versus R of different transmission distance for 64-QAM and the laser linewidth is 3 MHz.

TABLE 1. Complexity comparison between PDA-BPS and BPS algorithm for each symbol.

	Real Multiplication	Real Addition	Comparison	LUT
BPS	$55NB+2N$	$54NB-B+2N+22$	$16NB+B$	$2B+2$
PDA -BPS	$(55NB+2N)P+32$	$(54NB-B+2N+22)P+48$	$(16NB+B)P+16$	$(2B+2)P+16$

LUT: look-up table.

is mainly related to the number of symbols that do not enter the BPS algorithm, and has nothing to do with the modulation format. Complexity calculations are based on optimal implementations. For example, complex multiplication is composed of four real multiplications and two real additions, and complex addition is composed of two real additions. In Table 1, N is the smoothing filter length for sliding average methods set to 16. B is the number of test phase angles for PDA-BPS algorithm set to 18. $P = (N_1 - N_2)/N$, N_1 represents the total number of 32768 symbols, and N_2 represents the number of symbols that are not processed by the BPS algorithm, which determines the degree of complexity reduction of the proposed PDA-BPS algorithm. The size of N_2 is closely related to R. A larger R can effectively reduce the complexity of the algorithm, but it will sacrifice system performance. Figs. 10(a) and (b) shows BER as a function of R for different linewidths after 300 km transmission in the presence of three kinds of noise (EEPN, P2A noise, and ASE noise). The corresponding number of N_2 is given in Figs. 10(c) and (d). Fig. 11 shows the curve as the transmission distance changes. After weighing up the pros and cons of performance and complexity, R is set to 0.25 in this paper. Specifically, the complexity can be reduced by 40%/16.6% with 1 MHz/7 MHz linewidth for 16-QAM and 29%/10.9% with 0.5 MHz/3 MHz linewidth for 64-QAM.

IV. CONCLUSION

In this paper, the system model of complex-valued optical DSB transmission with CADD receiver under the influence of EEPN and P2A noise is proposed. The achievable performance of the complex-valued optical DSB transmission with CADD receiver is estimated by a closed-form expression, and it is verified by simulation that the results show an inaccuracy of less than 1 dB for a wide range of system parameters. Our work gives clear insights into the impact of the laser phase noise on CADD system, showing that both the EEPN and P2A have significant impact on the system performance. We have proposed and investigated the PDA-BPS algorithm to mitigate the effects of EEPN and P2A noise. The algorithm has comparable mitigation performance with the BPS algorithm while having lower complexity. Specifically, under the condition that R is equal to 0.25, the complexity can be reduced by 40%/16.6% with 1 MHz/7 MHz linewidth for 16-QAM and 29%/10.9% with 0.5 MHz/3 MHz linewidth for

64-QAM. We believe that the presented model can be used to accelerate the design and implementation of the CADD system for practical applications.

ACKNOWLEDGMENT

The authors would like to thank Prof. Weisheng Hu and Dr. Yixiao Zhu for their enthusiastic help.

REFERENCES

[1] Cisco. *Cisco Annual Internet Report (2018–2023)*. [Online]. Available: https://www.cisco.com/c/en/us/solutions/collateral/executiveperspectives/annual-internet-report/white-paper-c11-741490.html
[2] X. Li, S. An, H. Ji, J, Li, W, Shieh, and Y. Su, "Deep-learning-enabled high-performance full-field direct detection with dispersion diversity," *Opt. Exp.*, vol. 30, no. 7, pp. 11767–11788, Mar. 2022.
[3] I. Alimi, R. Patel, N. Silva, C. Sun, H. Ji, W. Shieh, and N. Muga, "A review of self-coherent optical transceivers: Fundamental issues, recent advances, and research directions," *Appl. Sci.*, vol. 11, no. 16, p. 7554, Aug. 2021.
[4] Q. Hu, K. Schuh, M. Chagnon, F. Buchali, and H. Bulow, "Up to 94 GBd THP PAM-4 transmission with 33 GHz bandwidth limitation," in *Proc. Eur. Conf. Opt. Commun. (ECOC)*, Sep. 2018, pp. 1–3.
[5] X. Chen, S. Chandrasekhar, J. Cho, and P. Winzer, "Single-wavelength and single-photodiode entropy-loaded 554-Gb/s transmission over 22-km SMF," in *Proc. Optical Fiber Commun. Conf.*, 2019, p. Th4B.5.
[6] X. Pang, O. Ozolins, R. Lin, L. Zhang, A. Udalcovs, L. Xue, R. Schatz, U. Westergren, S. Xiao, W. Hu, G. Jacobsen, S. Popov, and J. Chen, "200 Gbps/lane IM/DD technologies for short reach optical interconnects," *J. Lightw. Technol.*, vol. 38, no. 2, pp. 492–503, Jan. 15, 2020.
[7] C. Sun, H. Ji, T. Ji, Z. Xu, and W. Shieh, "Power loading for carrier assisted differential detection," in *Proc. Asia Commun. Photonics*, 2020, p. M3B.4.
[8] M. Qiu, Q. Zhuge, M. Y. S. Sowailem, T. M. Hoang, M. Chagnon, M. Xiang, X. Zhou, F. Zhang, and D. V. Plant, "Equalization-enhanced phase noise in Stokes-vector direct detection systems," *IEEE Photon. J.*, vol. 8, no. 6, pp. 1–7, Dec. 2016.
[9] X. Chen, S. Chandrasekhar, and P. Winzer, "Self-coherent systems for short reach transmission," in *Proc. Eur. Conf. Opt. Commun. (ECOC)*, Sep. 2018, pp. 1–3.
[10] D. Che, X. Chen, A. Li, Q. Hu, Y. Wang, and W. Shieh, "Optical direct detection for 100G short reach applications," in *Proc. Asia Commun. Photon. Conf.*, 2014, p. AF1H.4.
[11] D. Che, C. Sun, and W. Shieh, "Optical field recovery in Stokes space," *J. Lightw. Technol.*, vol. 37, no. 2, pp. 451–460, Jan. 15, 2019.
[12] D. Che, C. Sun, and W. Shieh, "Direct detection of the optical field beyond single polarization mode," *Opt. Exp.*, vol. 26, no. 3, pp. 3368–3380, Feb. 2018.
[13] M. Lyu, W. Shi, and L. A. Rusch, "SiP alternative to enhanced KK for OFDM," in *Proc. Eur. Conf. Opt. Commun. (ECOC)*, Sep. 2018, pp. 1–3.
[14] Y. Wen, A. Li, Q. Guo, Y. Cui, and Y. Bai, "200G self-homodyne detection with 64QAM by endless optical polarization demultiplexing," *Opt. Exp.*, vol. 28, no. 15, pp. 21940–21955, Jul. 2020.
[15] X. Chen, A. Li, D. Che, Q. Hu, Y. Wang, J. He, and W. Shieh, "Block-wise phase switching for double-sideband direct detected optical OFDM signals," *Opt. Exp.*, vol. 21, no. 11, pp. 13436–13441, Jun. 2013.
[16] L. Zhang, T. Zuo, Q. Zhang, E. Zhou, G. N. Liu, and X. Xu, "Transmission of 112-Gb/s+ DMT over 80-km SMF enabled by twin-SSB technique at 1550 nm," in *Proc. Eur. Conf. Opt. Commun. (ECOC)*, Sep. 2015, pp. 1–3.
[17] W. Shieh, C. Sun, and H. Ji, "Carrier-assisted differential detection," *Light, Sci. Appl.*, vol. 9, no. 1, p. 18, Feb. 2020.
[18] C. Sun, T. Ji, H. Ji, Z. Xu, and W. Shieh, "Experimental demonstration of complex-valued DSB signal field recovery via direct detection," *IEEE Photon. Technol. Lett.*, vol. 32, no. 10, pp. 585–588, May 15, 2020.
[19] Y. Zhu, L. Li, Y. Fu, and W. Hu, "Symmetric carrier assisted differential detection receiver with low-complexity signal-signal beating interference mitigation," *Opt. Exp.*, vol. 28, no. 13, pp. 19008–19022, Jun. 2020.
[20] T. Pfau, S. Hoffmann, and R. Noe, "Hardware-efficient coherent digital receiver concept with feedforward carrier recovery for M-QAM constellations," *J. Lightw. Technol.*, vol. 27, no. 8, pp. 989–999, Apr. 15, 2009.
[21] W. Shieh and K.-P. Ho, "Equalization-enhanced phase noise for coherent-detection systems using electronic digital signal processing," *Opt. Exp.*, vol. 16, no. 20, pp. 15718–15727, Sep. 2008.
[22] A. P. T. Lau, T. S. R. Shen, W. Shieh, and K.-P. Ho, "Equalization-enhanced phase noise for 100 Gb/s transmission and beyond with coherent detection," *Opt. Exp.*, vol. 18, no. 16, pp. 17239–17251, 2010.
[23] G. Jacobsen, M. Lidn, T. Xu, S. Popov, A. T. Friberg, and Y. Zhang, "Influence of pre- and post-compensation of chromatic dispersion on equalization enhanced phase noise in coherent multilevel systems," *J. Opt. Commun.*, vol. 32, no. 4, pp. 257–261, Jan. 2011.
[24] G. Jacobsen, T. Xu, S. Popov, J. Li, A. T. Friberg, and Y. Zhang, "EEPN and CD study for coherent optical nPSK and nQAM systems with RF pilot based phase noise compensation," *Opt. Exp.*, vol. 20, no. 8, pp. 8862–8870, Apr. 2012.
[25] A. Kakkar, R. Schatz, X. Pang, J. R. Navarro, H. Louchet, O. Ozolins, G. Jacobsen, and S. Popov, "Impact of local oscillator frequency noise on coherent optical systems with electronic dispersion compensation," *Opt. Exp.*, vol. 23, no. 9, pp. 11221–11226, 2015.
[26] A. Kakkar, J. R. Navarro, R. Schatz, H. Louchet, X. Pang, O. Ozolins, G. Jacobsen, and S. Popov, "Comprehensive study of equalization-enhanced phase noise in coherent optical systems," *J. Lightw. Technol.*, vol. 33, no. 23, pp. 4834–4841, Dec. 1, 2015.
[27] S. Yamamoto, N. Edagawa, H. Taga, Y. Yoshida, and H. Wakabayashi, "Analysis of laser phase noise to intensity noise conversion by chromatic dispersion in intensity modulation and direct detection optical-fiber transmission," *J. Lightw. Technol.*, vol. 8, no. 11, pp. 1716–1722, Nov. 1990.
[28] A. Yekani, S. Amiralizadeh, and L. A. Rusch, "Analytical study of optical SSB-DMT with IMDD," *J. Lightw. Technol.*, vol. 36, no. 3, pp. 666–674, Feb. 1, 2018.
[29] M. Zhu, J. Zhang, X. Huang, X. Yi, B. Xu, and K. Qiu, "Influence of EEPN and P2A noise with CD pre-and post-compensation in optical SSB transmission and Kramers-Kronig receiver system," *Opt. Exp.*, vol. 27, no. 14, pp. 19664–19674, Jul. 2019.
[30] S. T. Le, K. Schuh, and H. Nguyen Tan, "A closed-form expression for direct detection transmission systems with kramers-kronig receiver," *IEEE Photon. Technol. Lett.*, vol. 30, no. 23, pp. 2048–2051, Dec. 1, 2018.
[31] Y. Feng, L. Li, J. Lin, H. Xu, W. Zhang, X. Tang, L. Xi, and X. Zhang, "Joint tracking and equalization scheme for multi-polarization effects in coherent optical communication systems," *Opt. Exp.*, vol. 24, no. 22, pp. 25491–25501, Oct. 2016.

PENG QIN received the B.S. degree in communication engineering from Taishan University, in 2020, and the M.S. degree in electronic information engineering from Liaocheng University, Shandong, China, in 2023, where he is currently pursuing the Ph.D. degree in information and communication engineering. His research interests include short-reach self-coherent optical communications and advanced digital signal processing techniques.

CHENGLIN BAI (Senior Member, IEEE) is currently a second-class Professor. He has published more than 170 technical papers indexed by SCI and EI in the international recognized journals and conferences. He has also authored monographs. His current research interests include high-speed optical fiber communications, including novel transmission systems and advanced digital signal processing techniques. He is a Senior Member of OSA. He was awarded the second prize of the Ministry of Education Outstanding Scientific Research Achievement Award (Science and Technology Progress Award) and the two Shandong Science and Technology Awards (Natural Science Award).

QI QI received the B.S. degree from Liaocheng University, in 2020, where she is currently pursuing the M.S. degree in electronic information engineering. Her research interests include noise mitigation and equalization for optical communication systems.

HENGYING XU received the B.S. and M.S. degrees in electrical engineering from the Harbin University of Science and Technology, in 2003 and 2006, respectively, and the Ph.D. degree from the State Key Laboratory of Information Photonics and Optical Communications, Beijing University of Posts and Telecommunications. He is currently a Professor with the Shandong Provincial Key Laboratory of Optical Communication Science and Technology, Liaocheng University. He has published more than 70 related articles. His research interests include elastic optical networking and advanced digital signal processing techniques. He received a second-class Science and Technology Award from the China Ministry of Education.

FAN YANG received the B.S. degree from Liaocheng University, in 2020, where he is currently pursuing the M.S. degree. His research interests include advanced digital signal processing techniques and direct detection.

PENGFEI LI received the B.S. degree from the Dongchang College, Liaocheng University, Liaocheng, China, in 2018. He is currently pursuing the M.S. degree in optoelectronic information engineering with Liaocheng University. His research interest includes polarization multiplexed self-coherent optical communication systems.

YINING ZHANG received the B.S. degree in mathematics and applied mathematics from Liaocheng University, in 2003, and the M.S. degree in computational mathematics from Zhengzhou University, in 2006. He is currently an Associate Professor with Liaocheng University. His research interests include digital signal processing and machine learning.